Accepted to J. Chem. Phys. 10.1063/5.0149821

Size-Dependent Miscibility Controls the Kinetics of Anion Exchange in Cesium Lead Halide Nanocrystals

Dongyan Zhang[1], Xinyi Sarah Wu[1], Dong Wang[1], Bryce Sadtler[1,2]*

[1]Department of Chemistry, Washington University, St. Louis, Missouri 63130, United States

[2]Institute of Materials Science & Engineering, Washington University, St. Louis, Missouri 63130, United States

* To whom correspondence should be addressed. Email: sadtler@wustl.edu

Abstract

Anion exchange is a facile, post-synthetic method to tune the emission wavelength of colloidal cesium lead halide ($CsPbX_3$, X = Cl, Br, I) perovskite nanocrystals. While colloidal nanocrystals can exhibit size dependent phase stability and chemical reactivity, the role of size on the mechanism of anion exchange in $CsPbX_3$ nanocrystals has not been elucidated. We used single-particle fluorescence microscopy to monitor the transformation of individual $CsPbBr_3$ nanocrystals to $CsPbI_3$. By systematically varying the size of the nanocrystals and the concentration of substitutional iodide, we observed that smaller nanocrystals exhibit longer transition times in their fluorescence trajectories while larger nanocrystals undergo a more abrupt transition during anion exchange. Monte Carlo simulations were used to rationalize the size-dependent reactivity in which we varied how each exchange event affects the probability for further exchange. Greater cooperativity for simulated ion exchange leads to shorter transition times to complete exchange. We propose that size-dependent miscibility between $CsPbBr_3$ and $CsPbI_3$ at the nanoscale controls the reaction kinetics. Smaller nanocrystals maintain a homogeneous composition during anion exchange. As the nanocrystal size increases, variations in the octahedral tilting patterns of the perovskite crystals lead to different structures for $CsPbBr_3$ and $CsPbI_3$. Thus, an iodide-rich region must first nucleate within larger $CsPbBr_3$ nanocrystals, which is followed by rapid transformation to $CsPbI_3$. While higher concentrations of substitutional anions can suppress this size-dependent reactivity, the inherent differences in reactivity between nanocrystals of different sizes are important to consider when scaling up this reaction for applications in solid-state lighting and biological imaging.

Introduction

Colloidal semiconductor nanocrystals (NCs) exhibit size-dependent chemical and physical properties.[1-16] In addition to size-dependent shifts in their optical absorption and emission spectra, the relative stability of different crystalline phases and the kinetics and thermodynamics of transitions between phases in nanoscale crystals is size dependent. For example, the pressure needed to transform wurtzite CdSe NCs into rock salt increases as their size decreases due the lower surface energies of facets that comprise the initial wurtzite NCs relative to the rock salt phase and the increasing contribution of surface energy to the total energy of the crystals.[5-6, 8-9] More recently, size-dependent changes in the structure of cesium lead halide perovskite nanocrystals have been reported.[16] The cubic (α) and orthorhombic (γ) phases are the two main structures observed for perovskite $CsPbX_3$ NCs. Calculations using density functional theory indicate that the cubic perovskite phase becomes more stable than the orthorhombic phase as the nanocrystal size decreases due to the lower surface energy of the cubic phase.[17-18]

Lead halide perovskite semiconductors with the formula $APbX_3$ ($A = CH_3NH_3^+$ or Cs^+, $X = Cl^-$, Br^-, I^-) are promising candidates as the active material in solar cells, light-emitting diodes (LEDs), and other optoelectronic devices.[19-27] The high photoluminescence (PL) quantum yield, tunable bandgap, and solution-phase processing of $CsPbX_3$ nanocrystals make these materials attractive in light-emission applications.[28-34] Post-synthetic exchange of the halide anions in $CsPbX_3$ NCs produces solid solutions with tunable anion ratios (e.g., $CsPbBr_{3-x}I_x$ with $0 < x < 3$); the final anion composition is controlled by the relative concentrations of the substitutional and lattice halide anions.[29, 35-40] Since this reaction occurs within minutes at room temperature, anion exchange is an attractive method to control the bandgap and absorption and emission properties of cesium lead halide nanocrystals for optoelectronic devices.

Heterogeneity in the composition of $CsPbX_{3-x}Y_x$ solid solutions (where X and Y are two different halide anions) will lower the color purity of their emission, which is undesirable for LEDs incorporating these materials. Within a single crystal, the relative solid-state miscibility between halide anions determines the compositional homogeneity. $CsPbCl_3$ and $CsPbBr_3$ exhibit high miscibility and generally show high compositional uniformity following anion exchange.[35, 41] However, because of the larger difference in size and electronegativity between Br^- and I^- and the lower tolerance factors for perovskite $CsPbBr_3$ and $CsPbI_3$ crystals, this anion pair exhibits lower miscibility compared to the Cl/Br pair.[39, 42] For example, $CsPbBr_{3-x}I_x$ NCs produced by anion exchange of $CsPbBr_3$ NCs with PbI_2 were shown to possess a radial compositional gradient that is bromide rich at the core and iodide rich near the surface.[43]

Beyond heterogeneity within individual particles, variations in the size and shape of colloidal NCs prepared within the same batch along with differences in the local concentration of substitutional ions will lead to different rates of ion exchange among the NCs. Prior studies that monitor the ensemble emission wavelength or diffraction peaks of a large population of NCs have shown there are different stages of reaction during anion exchange.[39, 44-45] For example, different kinetics were observed for the transformation of $CsPbBr_3$ NCs to $CsPbCl_3$ compared with the transformation of $CsPbBr_3$ NCs to $CsPbI_3$; anion exchange was attributed to being diffusion-limited for the former but surface-limited for the latter.[44] However, because these measurements average over asynchronous changes in the transformation of many NCs, they obscure heterogeneity in the reactivity of individual NCs.

Single-particle measurements enable the quantification of how variations in the chemical and physical properties among different particles contribute to the ensemble behavior.[41, 46-66] In situ fluorescence microcopy has been used to monitor changes in the fluorescence intensity,

wavelength, and lifetime of individual semiconductor nanocrystals and microcrystals undergoing anion exchange, cation exchange, and ion intercalation.[41, 58-66] Measuring the fluorescence spectrum and/or fluorescence lifetime of a single NC during anion exchange provides information on how the photophysics of the semiconductor change with the extent of the reaction.[64-66] However, these measurements are generally limited to following only one particle at a time. On the other hand, by observing changes in fluorescence intensity, the transformation of hundreds of individual nanocrystals can be recorded simultaneously. Our previous work has used this method to monitor anion exchange between different $CsPbX_3$ (X = Cl, Br, I) NCs.[41, 63] In all cases, the time it takes a single NC to undergo ion exchange is much shorter than ensemble reaction rate. Each NC exhibits both a unique starting time to begin anion exchange (as determined by when the fluorescence intensity started to rise) and time to complete the transformation (as determined by when the fluorescence intensity plateaus). We thus assign a switching time to each single-particle fluorescence trajectory based on the rate of the intensity rise.

For different solid-state transformations, the concentration dependence of switching times has been shown to reflect the relative miscibility between the initial and final crystals. The switching time is independent of the concentration of the substitutional ions when the initial and final structures are immiscible (e.g., cation exchange between CdSe and Ag_2Se NCs and intercalation of $CH_3NH_3^+$ and Br^- into $PbBr_2$ NCs).[58, 62] In contrast, for highly miscible systems like anion exchange between $CsPbCl_3$ and $CsPbBr_3$ NCs, the switching times are strongly concentration dependent.[41] $CsPbBr_3$ and $CsPbI_3$ NCs exhibit intermediate miscibility between these extremes. We previously studied anion exchange between $CsPbBr_3$ and $CsPbI_3$ NCs using single-particle fluorescence and observed asymmetric behavior for the forward and backward exchange reactions (i.e., $CsPbBr_3$ to $CsPbI_3$ and vice versa).[63] We assigned this asymmetry to a smaller structural

reorganization that occurs when $CsPbBr_3$ NCs are converted to $CsPbI_3$ compared to exchange in the opposite direction (indicating the exchange reaction is irreversible). However, we only studied $CsPbBr_3$ NCs of a single size.

In this work, we synthesized $CsPbBr_3$ NCs with different average sizes to study the size-dependence of anion exchange to produce $CsPbI_3$ NCs. We used single-particle fluorescence microscopy to image the transformation of individual $CsPbBr_3$ NCs to $CsPbI_3$. We observe that smaller NCs exhibit a stronger concentration dependence of their switching times and longer switching times at lower concentrations of substitutional iodide compared to larger NCs. We used Monte Carlo methods to simulate anion exchange in individual particles and construct different models for how the particle size affects the probability for exchange. A larger amount of structural reorganization in a particle is reflected in a larger degree of positive cooperativity for successive exchange events, which leads to a smaller dependence of the switching time on the simulated concentration. By combining our experimental results with these simulations, we propose that smaller $CsPbBr_3$ NCs maintain a more homogenous structure and composition during anion exchange compared with larger NCs, which leads to longer transformation times once the reaction has started. On the other hand, the greater amount of structural reorganization needed for the transformation of larger NCs causes their switching times to be more abrupt. The insights gained from these studies inform the synthesis of $CsPbX_3$ NCs with uniform composition and emission wavelength. In the production of mixed-halide lead perovskite NCs via anion exchange, a high concentration of substitutional halide anions can suppress differences in the reactivity between nanocrystals of different sizes.

Results and Discussion

We first characterized the structural and ensemble optical properties of colloidal $CsPbBr_3$ nanocrystals (NCs) synthesized using a hot-injection method adapted from previous literature reports.[28, 67-68] Details of the synthesis are provided in the **Experimental section**. Representative transmission electron microscopy (TEM) images of $CsPbBr_3$ NCs with average edge lengths of 5.1 (11.8%), 6.1 (13.1%), 7.8 (15.4%), 9.5 (15.8%), and 13.1 (15.3%) nm are shown in **Figure 1** (the size dispersity for each sample measured by the standard deviation in edge lengths divided by the average edge length is given in parentheses). Histograms of the distribution of edge lengths for each NC size were fit to a normal distribution and are provided in **Figure S1** of the **Supplementary Material** (**SM**). The size dispersity increases as the average particle size increases, which occurs when the nucleation and growth of colloidal particles overlap in time[69] as has been observed for $CsPbBr_3$ NCs using the synthetic methods employed here.[70] The largest size of NCs also contained rectangular particles. The average edge length of the shorter edge was 13.1 nm, while the average edge length of the longer edge was 15.8 nm (for simplicity, this size will be referred to as 13.1-nm NCs as the optical spectra are determined by the shorter dimension).

Both the photoluminescence (PL) spectra (**Figure 2a**) and UV-visible absorption spectra (**Figure S2**) of the $CsPbBr_3$ NCs show size-dependent spectral shifts consistent with prior reports.[28-29, 44, 67-68, 71] Due to quantum confinement, both the PL emission maxima and the first-exciton absorption edges shift to shorter wavelengths as the average NC size decreases. **Table S1** in the **SM** provides the peak maxima and full widths at half maximum of the PL spectra. The peak positions of the PL spectra match previous reports for $CsPbBr_3$ NCs of different sizes (**Figure S3**).[44] The PL quantum yields of representative samples were around 40% (**Table S2**). X-ray diffraction (XRD) patterns indicate that all batches of $CsPbBr_3$ NCs possess the orthorhombic

perovskite structure (**Figure S4**). Broadening of the diffraction peaks was also observed as the NC size decreased as expected from Scherrer broadening when the number of lattice planes that contribute to diffraction for each peak in the XRD pattern decreases. This combined characterization shows we successfully controlled the size of $CsPbBr_3$ NCs by tuning the synthesis conditions and the washing process, which enables us to study the size dependence of anion exchange.

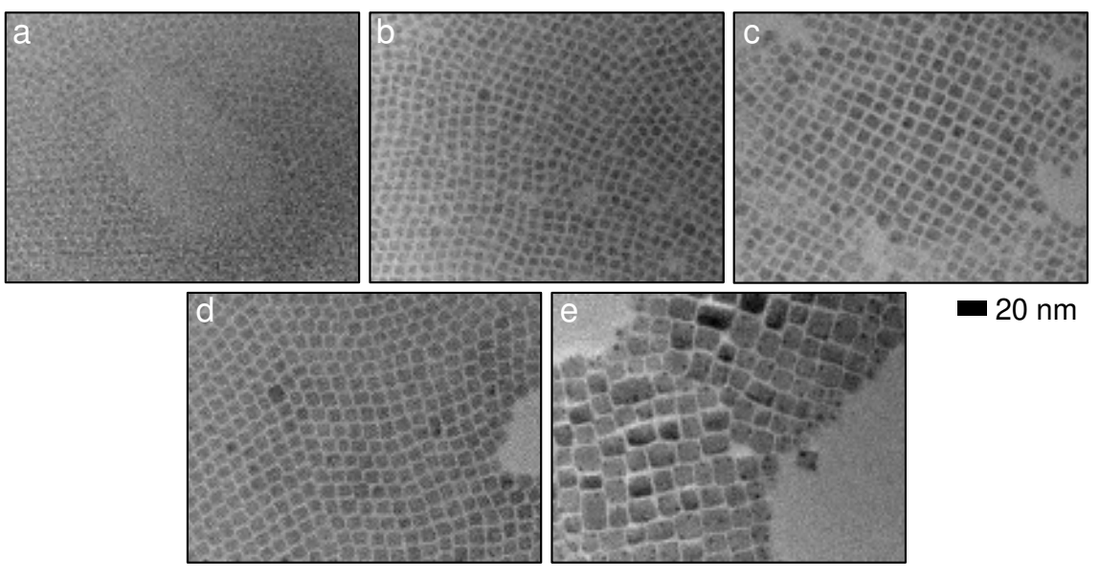

Figure 1. (a-e) TEM images of $CsPbBr_3$ NCs with different sizes. The average edge lengths ± the first standard deviation in the measured edge lengths of the NCs are (a) 5.1 ± 0.6 nm, (b) 6.1 ± 0.8 nm, (c) 7.8 ± 1.2 nm, (d) 9.5 ± 1.5 nm, and (e) 13.1 ± 2.0 × 15.8 ± 3.2 nm. Histograms of the size distribution for each batch of NCs are shown in **Figure S1**.

We next studied the transformation of $CsPbBr_3$ NCs to $CsPbI_3$ at the ensemble level using fluorescence spectroscopy. During anion exchange a solid solution between $CPbBr_3$ and $CsPbI_3$ is formed that can possess variable composition; the PL emission maxima shift to longer wavelengths

as the $CsPbBr_{3-x}I_x$ NCs become richer in iodide. Trimethylsilyl iodide (TMSI) was used as a precursor to convert $CsPbBr_3$ nanocrystals to $CsPbI_3$ via anion exchange. While we previously used tetrabutylammonium iodide to perform anion exchange in $CsPbBr_3$ NCs with an average edge length of 9.4 nm,[63] we found that this iodide precursor led to degradation in the smallest NC sizes studied here. TMSI dissolved in anhydrous hexane (i.e., the same solvent used to suspend the NCs) has been previously shown to significantly limit the degradation of $CsPbBr_3$ NCs during anion exchange to $CsPbI_3$.[40] The amount of TMSI added into a cuvette containing a solution of the $CsPbBr_3$ NCs in hexane was sufficient to provide an excess of iodide anions (see the **Experimental section** and **Figure S5** for details). Immediately after the addition of TMSI, the cuvette was shaken thoroughly, and fluorescence spectra were acquired every 35 seconds (i.e., the time it takes to collect a single spectrum). The time-dependent shifts in PL emission maxima for 5.1-nm $CsPbBr_3$ NCs after the addition of TMSI are shown in **Figure 2b**. The PL maximum of the initial $CsPbBr_3$ NCs was 486 nm, which shifted to 622 nm during the first 35 seconds of anion exchange. There is little change in the PL maxima after the first 35 seconds indicating that the exchange reaction has reached completion. A slight blue shift of the PL maxima to 615 nm occurred over a period of 315 seconds, which we attribute to etching of the NCs (see **Figure S6** for further details). The changes in PL emission maxima for 13.1-nm $CsPbBr_3$ NCs after TMSI addition are shown in **Figure 2c**. The emission maxima undergo a more gradual shift towards longer wavelengths compared to smaller NCs. Over a period of 1435 seconds, the maxima shift from 516 nm to 661 nm. While this method of observing the ensemble reaction rate is qualitative, the longer reactions times observed here for anion exchange of larger nanocrystals agree with previous reports using stop-flow techniques to quantitatively measure the ensemble-level reaction kinetics through the shift in PL spectra.[44] Additional characterization of the product $CsPbI_3$ NCs by energy dispersive

spectroscopy, TEM, absorption spectroscopy, and fluorescence spectroscopy are provided in **Table S3** and **Figures S7** through **S11** of the **SM**.

The type of ligands bound to the surface $CsPbX_3$ NCs can affect the rate of anion exchange.[72-73] Excess ligands in solution can also slow down the exchange reaction by binding to the substitutional halide ions. All batches of $CsPbBr_3$ NCs in this work were synthesized using oleylamine and oleic acid as ligands to stabilize the nanocrystals (see the **Experimental section** for further details). Excess oleylamine and oleic acid are removed during the washing steps following the synthesis of the $CsPbBr_3$ NCs. Furthermore, in the single-particle experiments described below, the flow cell is first flushed with pure hexane before the solution of TMSI is introduced. Thus, we do not expect differences in ligand binding to have a significant effect on the size-dependent reactivity observed in either ensemble fluorescence spectroscopy or single-particle fluorescence microscopy.

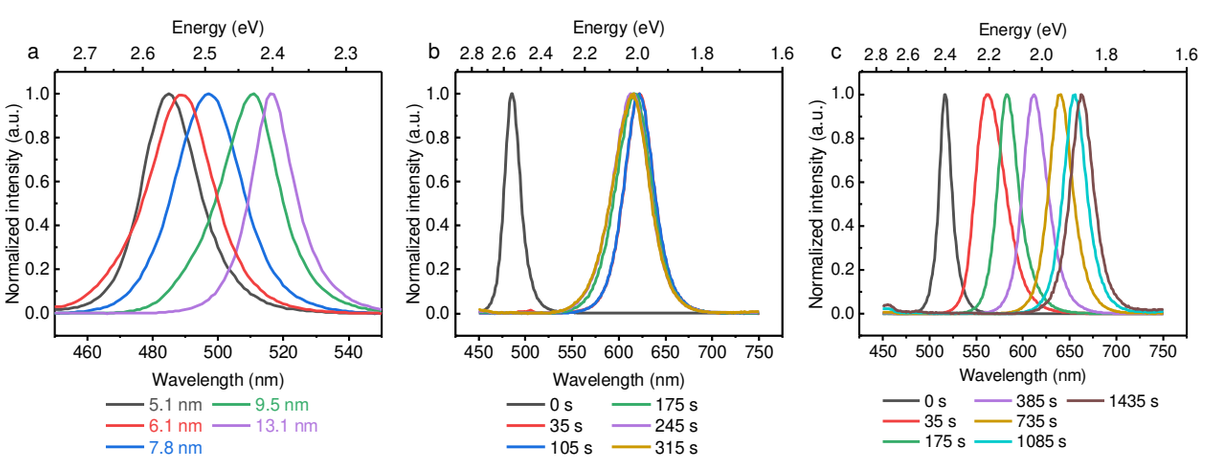

Figure 2. (a) PL spectra of different batches of $CsPbBr_3$ NCs showing size-dependent emission maxima. The spectra of the 6.1-nm and 7.8-nm samples were acquired using different batches of $CsPbBr_3$ NCs than those used for single-particle microscopy. They were prepared in the same way and showed nominally the same average edge length in their size histograms obtained by TEM.

(b) Time evolution of PL spectra for 5.1-nm $CsPbBr_3$ NCs after the addition of excess TMSI (0.01 M, 100 µL) to induce anion exchange. (c) Time evolution of PL spectra for 13.1-nm $CsPbBr_3$ NCs after the addition of excess TMSI (0.01 M, 100 µL). Only representative spectra are shown in plots (b) and (c) to avoid overlap of the spectra.

To determine how the NC size affects the mechanism of anion exchange, we monitored the transformation of $CsPbBr_3$ NCs to $CsPbI_3$ in situ at single-particle level with fluorescence microcopy. The assembly of flow cells and the setup for single-particle experiments are described in the **Experimental section** and in our previous work.[41, 62-63] A flow cell containing $CsPbBr_3$ NCs deposited on a microscope coverslip was placed on top of an inverted optical microscope, and a solution of TMSI was injected into the flow cell to induce anion exchange (**Figure 3a**). We chose a filter set that blocks emission from the initial $CsPbBr_3$ NCs but collects light emitted from iodide-rich $CsPbBr_xI_{3-x}$ NCs (**Figure S12**). As the emission from each NC shifts to longer wavelengths during anion exchange, they appear as bright spots within the microscope field-of-view (**Figure 3b, c**). Each reaction trajectory consists of the change in fluorescence intensity for a single particle with time (**Figure 4**). To exclude clusters of nanocrystals within a diffraction-limited spot, only fluorescence trajectories with clear "on" (i.e., emissive) and "off" (i.e., dark) states were included for subsequent analysis (see **Figures S13** and **S14** for examples), which is a signature of a single emitter. While time-correlated single-photon counting is needed to conclusively identify single emitters, our method enables us to collect the trajectories of hundreds of nanocrystals undergoing anion exchange at the same time and collect statistics for the reaction.

We define the incubation time as the time difference between when the TSMI solution first flows into the microscope field of view and when the fluorescence intensity starts to rise for the

ensemble of NCs. The incubation times when using a TMSI solution with a concentration of 5 µM were 393 s for 5.1-nm, 380 s for 6.1-nm, 393 s for 7.8-nm, 773 s for 9.5-nm and 891 s for 13.1-nm $CsPbBr_3$ NCs. Thus, larger NCs tend to exhibit longer ensemble incubation times for anion exchange consistent with the slower shifts in the maxima of the ensemble PL spectra shown in **Figure 2** (as the transforming NCs are not observed under the microscope until their emission wavelength falls within the window of the emission filter). Further analysis of the ensemble trajectories is limited because each single NC turns on at a different time. Thus, the integrated intensities (i.e., over the entire field of view) convolve differences in when the fluorescence trajectory for each NC starts with the steepness of its intensity rise.

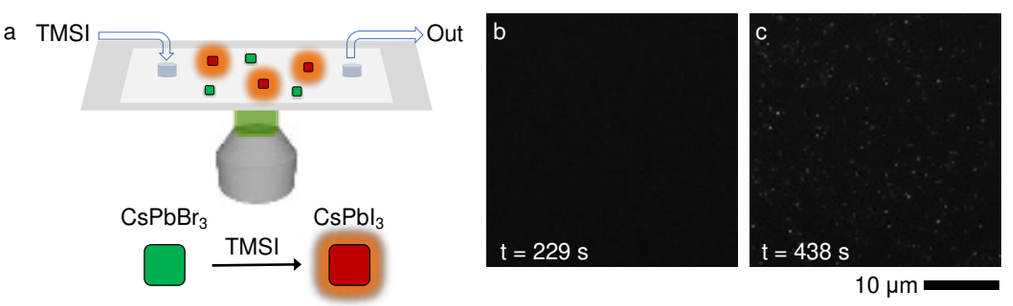

Figure 3. (a) Schematic of single-particle imaging of anion exchange using a flow cell placed over an inverted fluorescence microscope. The observation window of the emission filter is 590 – 649 nm (**Figure S12**). (b) Snapshot (t = 229 s, measured from when the injection of TMSI into the flow cell started) from a fluorescence video before the transformation of 13.1-nm $CsPbBr_3$ NCs. (c) Snapshot (t = 438 s) from the same fluorescence video showing the fluorescence intensity after the transformation of the NCs to $CsPbI_3$. The TMSI concentration used to induce the transformation was 12.5 µM. The background brightness of each snapshot was set to same intensity.

Our prior work has shown that the steepness of the fluorescence intensity rise of individual NCs during anion exchange is an important parameter in extracting mechanistic information for the solid-state transformation.[41, 62-63] We next examined how the concentration of TMSI and the size of the nanocrystals affect this parameter. Representative single-particle reaction trajectories from the batches of $CsPbBr_3$ NCs with the smallest and largest average sizes (i.e., 5.1 and 13.1 nm) and using the lowest and highest TMSI concentrations (i.e., 5 and 50 μM) to induce anion exchange are shown in **Figure 4**. For both sizes, the intensity change during the transformation rises more steeply using the higher TMSI concentration. For the same TMSI concentration, smaller NCs undergo a more gradual increase in intensity while the larger NCs exhibit a steeper rise in their intensity trajectory during anion exchange.

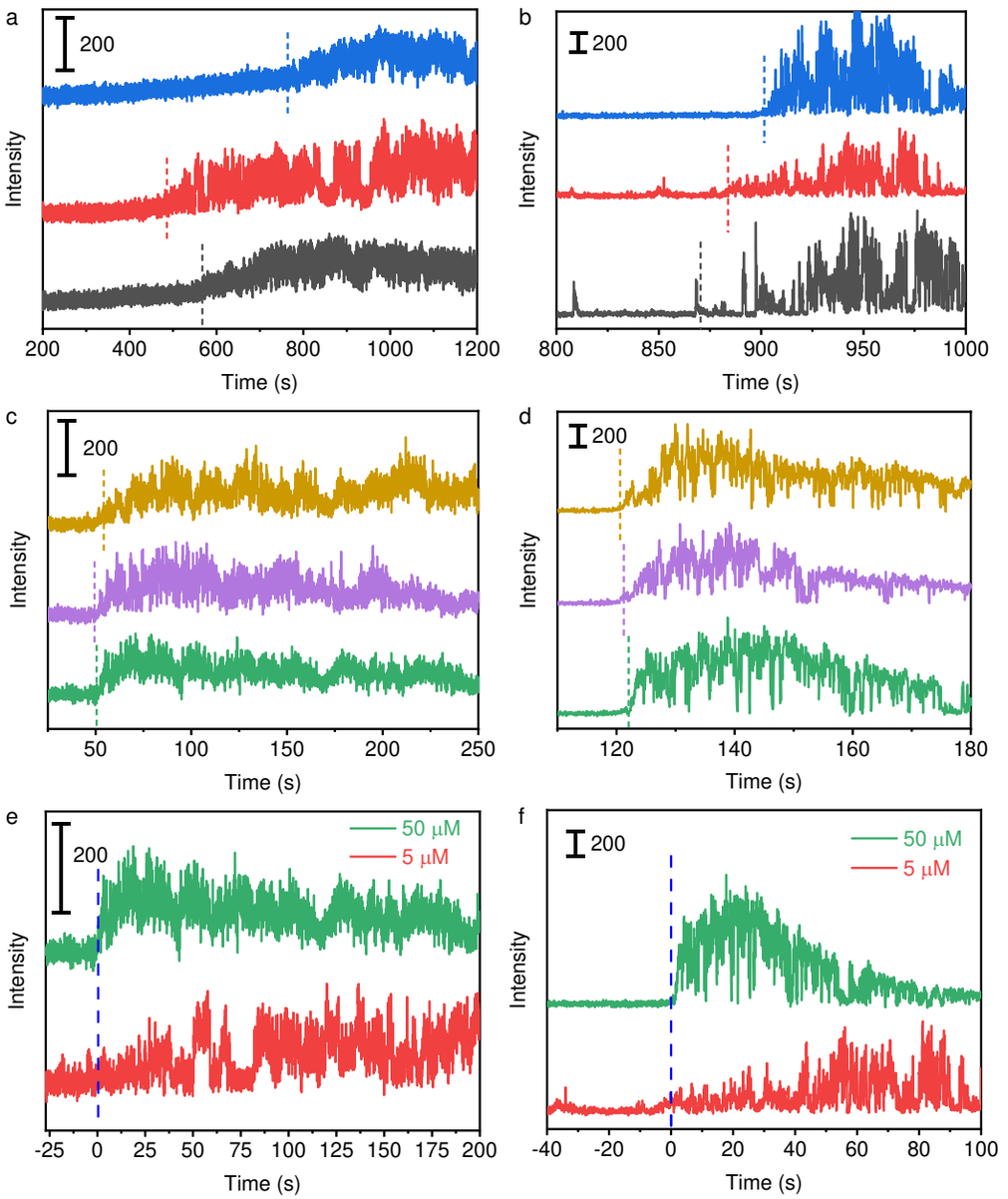

Figure 4. Representative single-particle fluorescence trajectories during anion exchange of $CsPbBr_3$ NCs to $CsPbI_3$. (a) Trajectories of 5.1-nm $CsPbBr_3$ NCs transformed using a TMSI solution with a concentration of 5 μM. (b) Trajectories of 13.1-nm $CsPbBr_3$ NCs transformed using a TMSI solution with a concentration of 5 μM. (c) Trajectories of 5.1-nm $CsPbBr_3$ NCs transformed using a TMSI solution with a concentration of 50 μM. (d) Trajectories of 13.1-nm $CsPbBr_3$ NCs transformed using a TMSI solution with a concentration of 50 μM. Panels (e) and

(f) compare trajectories at different TMSI concentrations. (e) Trajectories of 5.1-nm $CsPbBr_3$ NCs transformed using TMSI solutions with concentrations of 5 µM (red, middle trace in panel a) and 50 µM (green, bottom trace in panel c). (f) Trajectories of 13.1-nm $CsPbBr_3$ NCs transformed using TMSI solutions with concentrations of 5 µM (red, middle trace in panel b) and 50 µM (green, bottom trace in panel d). The vertical dashed lines indicate where the single-particle trajectories start to rise (set to 0 in panels e and f for comparison). After reaching their maximum, the PL intensity of the NCs decrease due to degradation when using TMSI with a concentration of 50 µM. The vertical scale bars in each panel provide the intensity scale (in arbitrary intensity units). The 13.1-nm NCs exhibit higher fluorescence intensities during the transformation due to their larger volume and absorption cross-section.

To quantify the steepness of the intensity rise for individual NCs, we fit each reaction trajectory to a sigmoidal function and extracted a switching time based on the fit (see the **SM** for details and **Figure S15** for examples of the sigmoidal fits). A shorter switching time indicates a steeper rise in intensity. We performed single-particle fluorescence microscopy on each batch of NCs using TMSI concentrations of 5, 7.5, 10, 12.5, 15, 20, 30, and 50 µM to induce anion exchange. For each average size and TMSI concentration, we fit over 250 individual reaction trajectories. At the flow rate used to inject the TMSI solution (20 mL/h), the switching times did not show any dependence on the location of the nanocrystal within the microscope field of view (**Figure S16**). The mean switching times for each condition are shown in **Figure 5a** (see also **Figure S17** in the **SM** for an expanded view of the switching times at low TMSI concentrations). For each batch of NCs, the average switching time decreases as the concentration of TMSI increases. We note that the exchange reaction initiates before emission from the $CsPbBr_{3-x}I_x$ NCs comes into view with the

filter set used. For the portion of the exchange reaction that we observe, two important trends emerge as can be seen in **Figure 5a**. 1) Smaller NCs exhibit longer switching times during anion exchange. 2) The switching times of smaller NCs exhibit a stronger concentration dependence (i.e., the switching times increase more steeply at lower TMSI concentrations). For example, as the concentration of TMSI increases from 5 µM to 50 µM, the mean switching time (± first standard deviation) decreases from 135.6 ± 37.3 s to 18.1 ± 9.4 s for the 5.1-nm NCs. For the 13.1-nm NCs, the mean switching time decreases from 14.1 ± 8.1 s to 2.7 ± 1.8 s over this concentration range. This unexpected behavior indicates that the reaction path for anion exchange is size dependent.

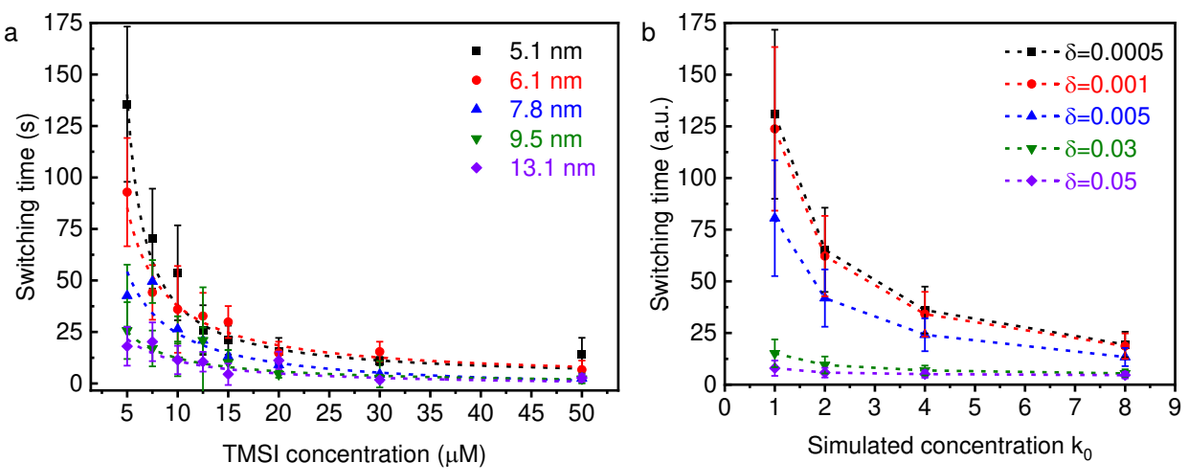

Figure 5. Comparison of experimental and simulated switching times for anion exchange of $CsPbBr_3$ NCs. (a) Concentration dependence of experimental switching times for $CsPbBr_3$ NCs with different sizes. Each data point represents the mean switching time from fitting the trajectories of at least 250 NCs. The TMSI concentrations used for each NC size were: 5, 7.5, 10, 12.5, 15, 20, 30, and 50 µM. (b) Simulated switching times for different values of cooperativity, δ, and concentration, k_0. Each data point represents the mean of simulated trajectories from 500 particles.

The dashed lines in both panels are guides to the eye. The error bars for each data point in both plots indicate the standard deviation in the experimental/simulated switching times.

We used Monte Carlo methods to model differences in the reaction path for particles of different sizes. The main parameter we varied in these simulations is how the reaction barrier changes for consecutive exchange events in a particle during anion exchange (see the **SM** for details of the simulations). Cooperativity in the solid-state transformation was modeled by a change in free energy that decreases with successive exchange events and thus a probability for exchange that increases with successive exchange events. Systems in which the initial and final crystals exhibit a larger difference in structure have been shown to exhibit greater cooperativity during the transformation of the nanocrystal. Previous work by us and others has shown that stronger cooperativity leads to sharper transitions and shorter switching times in the simulated trajectories for ion exchange.[41, 58, 62-63] Stronger cooperativity also makes the switching times relatively insensitive to the concentration of substitutional ions.

In our previous work, we used single-particle fluorescence to monitor anion exchange in $CsPbBr_3$ NCs with an average size of 9.4 nm.[63] A model where the change in free energy for exchange events decreased quadratically with the number of events reproduced the concentration dependence of switching times for this size of NCs.

$$\Delta G_i = \Delta G_0 - \delta i^2$$

Where i is the number of exchange events in a particle, ΔG_i is the change in free energy for the i^{th} exchange event, and ΔG_0 and δ are empirical constants. We adapted this model by varying the value of δ, which determines the degree of cooperativity during the simulation. As δ increases, the degree of cooperativity increases, and the probability for further exchange increases more

rapidly as the reaction progresses (**Figure S18**). For each value of δ, the value of ΔG_0 was varied to simulate different concentrations of substitutional iodide (see the **SM** for details). Simulated reaction trajectories for different values of δ are shown in **Figure S19**. As the value of δ increases, the trajectories of individual particles become increasingly sharper relative to the ensemble trajectory. The mean switching times for the simulations are shown in **Figure 5b**. Switching times for additional values of δ are shown in **Figure S20**. The values of δ shown in **Figure 5b** were chosen as they exhibit qualitatively similar concentration dependences to the experimental data. Larger values of δ lead to shorter switching times and switching times that are relatively insensitive to the simulated concentration of substitutional iodide. Based on the comparison of these simulations to experimental switching times determined by single-particle fluorescence, we associate stronger cooperativity with the transformation of larger $CsPbBr_3$ NCs.

Our results can be rationalized by a size-dependent miscibility between $CsPbBr_3$ and $CsPbI_3$ crystals at the nanoscale. Calculations using density functional theory indicate that the cubic perovskite phase becomes thermodynamically stable in both $CsPbBr_3$ and $CsPbI_3$ for small crystal sizes (e.g., edge lengths ranging from 2.7 to 10 nm for $CsPbI_3$ and from 9.7 to 48.3 nm for $CsPbBr_3$ depending on the calculation).[17-18] Rather than a distinct phase transition between the cubic and orthorhombic perovskite phases of $CsPbI_3$, Zhao and coworkers have shown that the lattice constants and tilting of PbI_6 octahedra vary continuously for NCs in the size range of 5 to 15 nm.[16] Larger $CsPbI_3$ NCs possess the orthorhombic structure. As the NC size decreases, surface strain causes the lattice volume to expand while the degree of octahedral tilting decreases such that smaller NCs are more cubic like. Such measurements have not been performed on $CsPbBr_3$ NCs. However, due to their different surface energies[18] and anion radii (1.82 Å for Br^- and 2.06 Å for I^-), we hypothesize that the degree of size-dependent octahedral tilting will be different between

$CsPbBr_3$ and $CsPbI_3$. Our previous experiments show that switching times observed by single-particle microscopy become shorter and less sensitive to the concentration of substitutional ions as the difference between the structures of the initial and final crystals becomes greater (i.e., as the miscibility between initial and final crystals decreases).[41, 62-63] Thus, our results are consistent with higher miscibility between $CsPbBr_3$ and $CsPbI_3$ for smaller sizes when their crystal structures are more cubic like. The miscibility decreases for larger NC sizes due to changes in the tilting patterns of the PbX_6 octahedra that differ for the orthorhombic perovskite phases of these two materials.

A larger difference between the structures of $CsPbBr_3$ and $CsPbI_3$ for larger NC sizes requires more substantial structural reorganization during anion exchange. Smaller $CsPbBr_3$ NCs can maintain a homogeneous structure during anion exchange, consistent with the longer switching times and the stronger concentration dependence of switching times. The higher surface-to-volume ratio and shorter diffusion distances for exchange in smaller NCs also facilitate a homogeneous composition while anions are diffusing in and out.[43, 74] On the other hand, our results indicate that larger $CsPbBr_3$ NCs require nucleation of an iodide-rich phase within the $CsPbBr_3$ NCs. Once the iodide-rich phase has formed, lattice strain between the bromide-rich and iodide-rich regions creates a driving force for the NC to completely transform to $CsPbI_3$ (thus leading to the stronger cooperativity). This mechanism is consistent with the shorter switching times, particularly at low concentrations of TMSI that we observe as the size of the $CsPbBr_3$ NCs increases. This mechanism is also consistent with the Monte Carlo simulations that show a higher degree of cooperativity is associated with a larger amount of structural reorganization. Finally, these results are consistent with previously reported time-correlated, single-photon counting of $CsPbBr_3$ NCs during anion exchange to $CsPbI_3$. Masuo and coworkers showed that $CsPbBr_3$ NCs with an average size of 7.8 nm behaved as single-photon emitters during anion exchange to $CsPbI_3$, indicating a homogenous

structure throughout the reaction.[64] When this group performed the same studies on $CsPbBr_3$ NCs with an average size of 19.0 nm, they observed a change in the number of emission sites during anion exchange,[66] which they attributed to the presence of distinct iodide-rich and bromide-rich regions within the NC during anion exchange.

Conclusions

This work demonstrates that the size-dependent structure of lead halide perovskite nanocrystals impacts their chemical reactivity. Through single-particle fluorescence microscopy, we observe shorter switching times during the transformation of larger $CsPbBr_3$ NCs to $CsPbI_3$ via anion exchange. Monte Carlo simulations support a more abrupt change in structure after the anion exchange reaction initiates for larger NCs, which requires nucleation of a new phase and leads to greater cooperativity in the transformation. On the other hand, smaller NCs can maintain a homogenous composition and structure during the exchange reaction leading to longer switching times at lower concentrations of substitutional halide ions. While our results show that batches of colloidal nanocrystals with different average sizes exhibit different reactivity, there is significant heterogeneity within each batch in the switching times of individual nanocrystals (the vertical lines in **Figure 5a** show the standard deviation in mean switching times). Our results suggest that the variations in switching times for anion exchange within a sample are due in part to the dispersity in size of the nanocrystals. This heterogeneity is important to consider when scaling up the production of cesium lead halide nanocrystals for incorporation into optoelectronic devices. Variations in the size of the nanocrystals can not only broaden the range of emission wavelengths due to quantum-confinement effects, but they can also lead to different reactivity (and thus variations in

composition) for individual nanocrystals when targeting a specific composition and emission wavelength through anion exchange.

Additionally, defects in colloidal semiconductor nanocrystals will affect optical properties, such as their photoluminescence quantum yield. By monitoring the fluorescence intensity trajectories of individual nanocrystals, one could track how their reactivity during anion exchange correlates with their fluorescence intermittency, which provides a signature of trap states within the band gap of the nanocrystals. Future work includes understanding how the size-dependent miscibility and switching times affect the presence and distribution of defects introduced during anion exchange.

Supplementary Material. See the supplementary material for experimental details on sample characterization by XRD, energy dispersive x-ray (EDX) spectroscopy, and quantum yield measurements, analysis of fluorescence videos, and Monte Carlo simulations; supplementary tables providing the maxima in the PL spectra and their full width at half-maximum for $CsPbBr_3$ NCs with different sizes, PL quantum yields of $CsPbBr_3$ NCs, and compositional analysis by EDS spectroscopy before and after anion exchange; supplementary figures showing size distributions of the $CsPbBr_3$ NCs, UV-visible absorption spectra, PL maxima as a function of NC size, and XRD patterns of $CsPbBr_3$ NCs, PL spectra after aliquots of TMSI were added to the $CsPbBr_3$ NCs, PL spectra of different batches of $CsPbBr_3$ NCs, scanning transmission electron microscopy images, size distributions, PL spectra, and absorbance spectra of the product $CsPbI_3$ NCs prepared by anion exchange, transmittance spectra of the filter set used for single-particle fluorescence microscopy, examples of fitting single-particle fluorescence trajectories to a sigmoidal function, a comparison of the intensity trajectories for single NCs and clusters of NCs, switching times for

different NCs as a function of their position in the field of view, expanded view of the experimental switching times at low TMSI concentrations, simulated changes in free energy and probability for anion exchange for different degrees of cooperativity, simulated trajectories for anion exchange, and simulated switching times for additional degrees of cooperativity.

Author Contributions.

Dongyan Zhang: Investigation (lead), Formal analysis (lead), Software (lead), Writing (equal),

Xinyi Sarah Wu: Investigation (supporting), Formal analysis (supporting)

Dong Wang: Investigation (supporting), Software (supporting)

Bryce Sadtler: Conceptualization (lead), Supervision (lead), Funding acquisition (lead), Writing (equal)

Acknowledgements.

This material is based upon work supported by the National Science Foundation (NSF) under grant no. CHE-1753344 to B.S. X.S.W. acknowledges support from Washington University for a Summer Undergraduate Research Award. Electron microscopy was performed at the Institute of Materials Science & Engineering at Washington University. X-ray diffraction was performed in the Department of Earth and Planetary Sciences at Washington University. The authors thank Jiang Luo for assistance with EDX spectroscopy, Huafang Li for assistance with electron microscopy, and Rena Kramer for assistance with measuring PL quantum yields.

Conflict of interest statement. The authors have no conflicts to disclose.

Data availability statement. The data that support the findings of this study are available from the corresponding author upon reasonable request.

Experimental section

Materials

The following chemicals were used as received: cesium carbonate (Cs_2CO_3, 99%, Millipore Sigma Inc.), lead(II) bromide ($PbBr_2$, > 98%, Alfa Aesar), oleic acid (OA, 90%, Millipore Sigma Inc.), oleylamine (OAm, 70%, Millipore Sigma Inc.), hexane (anhydrous, 95%, Millipore Sigma Inc.), 1-octadecene (ODE, tech. 90%, Alfa Aesar), trimethylsilyl iodide (TMSI, 97%, Millipore Sigma Inc.), acetone (HPLC, 99.8%, Millipore Sigma Inc.). TMSI was stored at –20°C in a built-in refrigerator inside a nitrogen-filled glovebox. The bottle of TMSI was used within one month after opening it to minimize degradation.

Synthesis of $CsPbBr_3$ nanocrystals with average edge length of 9.5 nm

All flasks used to synthesize $CsPbBr_3$ nanocrystals were stirred at 400 rpm using a magnetic stir bar and stirring plate to dissolve and mix the reagents. The synthesis of $CsPbBr_3$ NCs with an average edge length of 9.5 nm was adapted from the procedure of Kovalenko et al.,[28] with modifications as follows. To prepare the Cs-oleate precursor solution, 0.102 g of Cs_2CO_3 was added to a mixture of 0.312 mL of OA and 5 mL of ODE in a 50-mL, round-bottom flask (labeled as Flask I). To prepare the lead bromide precursor, 0.069 g of $PbBr_2$ was added to a mixture of 1 mL of OA, 1 mL of OAm, and 5 mL of ODE in a second 50-mL, round-bottom flask (labeled as Flask II). Both flasks were heated at 120°C under vacuum for 30 min. The temperature of Flask I was then raised to 150°C while that of Flask II remained at 120°C under argon (95%) for another

30 min. Next, 0.4 mL of the solution from Flask I was swiftly injected into Flask II. After 1 min, Flask II was quenched in an ice bath. The mixture in Flask II was then transferred to a centrifuge tube and centrifuged at 8000 rpm for 5 min. The precipitate was collected, transferred into a glovebox, and dispersed in 10 mL of hexane.

Synthesis of $CsPbBr_3$ nanocrystals with average edge lengths of 5.1, 6.1, and 7.8 nm

To prepare $CsPbBr_3$ NCs with average sizes smaller than 9.5 nm, we adapted the procedure from Son et al.,[67] with modifications as follows. For the Cs-oleate solution, 0.125 g of Cs_2CO_3 was dissolved in a mixture of 0.447 mL of OA and 4.436 mL of ODE in a 50-mL, round-bottom flask (labeled as Flask I). To prepare the lead bromide precursor, 0.074 g of $PbBr_2$ and varying amounts of $ZnBr_2$ were added into a mixture of 1 mL of OA, 1 mL of OAm, and 5 mL of ODE in a second 50-mL, round-bottom flask (labeled as Flask II). The amounts of $ZnBr_2$ were 0.184 g, 0.530 g, and 0.530 g to produce $CsPbBr_3$ NCs with average edge lengths of 5.1, 6.1, and 7.8 nm, respectively. Both flasks were heated at 120°C under vacuum for 30 min. Flask I was then heated to 150°C under Ar while Flask II was maintained at 120°C under Ar for another 30 min. Before injection of the Cs-oleate precursor, Flask II was heated to either 140°C (for 5.1-nm NCs) or 190°C (for 6.1- and 7.8-nm NCs). Then, 0.2 mL of the solution from Flask I was injected swiftly into Flask II. After different reaction times (88 s for 5.1-nm NCs, 10 s for 6.1-nm NCs, and 10 s for 7.8-nm NCs), Flask II was quenched in an ice bath.

For the batches of $CsPbBr_3$ NCs with average sizes of 5.1 and 6.1 nm, the washing procedure is as follows. After cooling, the mixture in Flask II was transferred to a centrifuge tube and centrifuged at 3500 rpm for 10 min to remove unreacted salts. The supernatant was collected, and the precipitate was discarded. As an antisolvent, 8 mL of acetone was then added to the supernatant

and mixed thoroughly. The mixture was centrifuged at 3500 rpm for 3 min. The precipitate was collected, transferred into a glovebox, and dispersed in 10 mL of hexane. For the batch of $CsPbBr_3$ NCs with an average size of 7.8 nm, the mixture after synthesis was transferred to a centrifuge tube and centrifuged at 8000 rpm for 5 min. The precipitate was collected, transferred into a glovebox, and 10 mL hexane was added to disperse the precipitate. The mixture was centrifuged again at 3500 rpm for 3 min to remove unreacted salts. The supernatant was collected and transferred into a glovebox.

Synthesis of $CsPbBr_3$ nanocrystals with average edge length of 13.1 nm

The synthesis of $CsPbBr_3$ NCs with an average edge length of 13.1 nm was adapted from the step-growth method reported by Xie, Pradhan, et al.[68] For the Cs-oleate solution, 0.131 g of Cs_2CO_3 was dissolved in a mixture of 0.5 mL of OA and 3.2 mL of ODE in a 50-mL, round-bottom flask (labeled as Flask I). To prepare the lead bromide precursor, 0.0734 g of $PbBr_2$ was added to a mixture of 0.5 mL of OA, 0.5 mL of OAm, and 3.5 mL of ODE in a second 50-mL, round-bottom flask (labeled as Flask II). Flask I was maintained at 120°C under vacuum for 1 h and then heated to 150°C under Ar until the mixture turned clear. Flask II was maintained at 150°C under vacuum for 30 min and then under Ar until the mixture turned clear. The mixture in Flask II was then cooled down to 25°C. Next, 0.2 mL of the mixture in Flask I was injected into Flask II. After reacting for 30 minutes while stirring, the mixture was centrifuged at 10,000 rpm for 10 min. The precipitate was collected, transferred into a glovebox, and dispersed in 2 mL of ODE to prepare a seed solution for further growth.

In a third 50-mL, round-bottom flask (labeled as Flask III), 4 mL of ODE was maintained at 25°C under vacuum for 10 min. The atmosphere was then switched to Ar while 2 mL of the seed

solution was injected into Flask III. The mixture was heated to 200°C with a heating rate of approximately 10°C/min. After the temperature reached 200°C, the mixture was cooled in an ice bath to room temperature, transferred to a centrifuge tube, and then centrifuged at 10,000 rpm for 10 min. The precipitate was collected, transferred into a glovebox, and dispersed in 10 mL of hexane.

Optical spectroscopy

Photoluminescence (PL) spectra were measured using a Cary Eclipse fluorescence spectrophotometer. The excitation wavelength was 400 nm, and the step size was 1 nm. The entrance slit was set to 5 nm. The exit slit was varied between 2.5, 5, and 10 nm depending on the emission intensity of the sample. To prepare each sample for PL spectroscopy, the original solution of $CsPbBr_3$ NCs was diluted 200 times with hexane and transferred to a quartz cuvette. The time evolution of PL spectra for a given sample during anion exchange was measured by adding 100 µL of a 0.01 M solution of TMSI in hexane to the cuvette and running a PL scan every 35 seconds. This concentration of TMSI provides an excess of iodide relative to the total amount of bromide in the $CsPbBr_3$ sample. Titrations of the amount of TMSI needed for anion exchange to be complete were determined by sequentially adding 20-µL aliquots of a 0.001 M solution of TMSI in hexane to the cuvette containing $CsPbBr_3$ NCs in hexane. After each addition of TMSI, the cuvette was shaken thoroughly for 30 seconds, and a PL spectrum was acquired. Only representative spectra are plotted in **Figure S5** for the titration experiments of each NC size.

UV-Vis absorption spectra were measured using a Cary 60 spectrometer. The scan range was from 800 nm to 200 nm. To prepare each sample for absorption spectroscopy, the original $CsPbBr_3$ NC solution was diluted 50 times with hexane and transferred to a quartz cuvette.

Single-particle fluorescence microscopy

To prepare flow cells to image anion exchange using single-particle fluorescence microscopy, diluted solutions of the $CsPbBr_3$ NCs were spin-coated onto microscope coverslips. Two holes were drilled into a separate glass slide using a Dremel, which was then attached to the microscope coverslip using epoxy to make the flow cell. Additional details on the preparation of flow cells are provided in our previous reports.[41, 62-63]

The flow cell was placed on the stage of an inverted fluorescence microscope with the coverslip containing the NCs on the bottom. Fluorescence microscopy was performed using a Nikon N-STORM microscopy system consisting of a Nikon TiE motorized inverted optical microscope and a Nikon CFI-6-APO TIRF 100× oil-immersion objective lens with a numerical aperture of 1.49 and a working distance of 210 μm. An X-cite 120 LED system with a light intensity of ~29 $\mu W/cm^2$ at the focal plane was used as excitation source. The flow cell was first filled with pure hexane using a syringe pump. The top of the coverslip with deposited $CsPbBr_3$ NCs was brought into focus using a green filter set (Chroma #49002-ET-EGFP, excitation window: 450 – 490 nm, emission window: 500 – 540 nm). A second syringe pump was used to inject a TMSI solution into the flow cell to induce anion exchange. The flow rate was fixed at 20 mL/h based on our prior work.[63] The concentrations of TMSI solutions used were 5, 7.5, 10, 12.5, 15, 20, 30, 50 μM. To monitor anion exchange of single $CsPbBr_3$ nanocrystals, a red filter set (Chroma #49005-ET-DSRed, excitation window: 530−558 nm, emission window: 590−649 nm) was used to observe the emission from $CsPbBr_{3-x}I_3$ nanocrystals during anion exchange. Under these conditions, the background is initially dark as the emission filter cut offs the emission from the $CsPbBr_3$ NCs. The emission of individual $CsPbBr_{3-x}I_3$ NCs shifts to longer wavelengths as they become richer in

iodide, leading to an increase in their fluorescence intensity. An Andor iXon 897 electron-multiplying CCD camera (512 × 512, 16 μm pixels, > 90% quantum efficiency) was used to detect fluorescence signals. The exposure time was set to 50 ms.

Transmission electron microscopy (TEM) & scanning transmission electron microscopy (STEM)

Bright-field TEM and high-angle annular dark-field (HAADF) STEM images were acquired by using a JEOL 2100F TEM operated at an acceleration voltage of 200 kV. An aliquot of the solution of $CsPbBr_3$ NCs was diluted approximately 10 times with hexane. Then, 20 μL of the diluted solution was drop cast onto a copper TEM grid in a glovebox and allowed to dry at room temperature. To image $CsPbI_3$ NCs produced by anion exchange using STEM, 500 μL of a solution of $CsPbBr_3$ NCs was mixed with 500 μL of a 0.01 M solution of TMSI in hexane. The solution was diluted approximately 10 times with hexane before drop casting an aliquot of the solution onto a TEM grid.

References

1. Rossetti, R.; Nakahara, S.; Brus, L. E., Quantum Size Effects in the Redox Potentials, Resonance Raman Spectra, and Electronic Spectra of CdS Crystallites in Aqueous Solution. *The Journal of Chemical Physics* **1983,** *79*, 1086-1088.
2. Goldstein, A. N.; Echer, C. M.; Alivisatos, A. P., Melting in Semiconductor Nanocrystals. *Science* **1992,** *256*, 1425-1427.
3. Murray, C. B.; Norris, D. J.; Bawendi, M. G., Synthesis and Characterization of Nearly Monodisperse CdE (E = Sulfur, Selenium, Tellurium) Semiconductor Nanocrystallites. *Journal of the American Chemical Society* **1993,** *115*, 8706-8715.
4. Dabbousi, B. O.; Rodriguez-Viejo, J.; Mikulec, F. V.; Heine, J. R.; Mattoussi, H.; Ober, R.; Jensen, K. F.; Bawendi, M. G., (CdSe)ZnS Core−Shell Quantum Dots: Synthesis and Characterization of a Size Series of Highly Luminescent Nanocrystallites. *The Journal of Physical Chemistry B* **1997,** *101*, 9463-9475.
5. Tolbert, S. H.; Alivisatos, A. P., Size Dependence of a First Order Solid-Solid Phase Transition: The Wurtzite to Rock Salt Transformation in CdSe Nanocrystals. *Science* **1994,** *265*, 373-376.
6. Tolbert, S. H.; Alivisatos, A. P., The Wurtzite to Rock Salt Structural Transformation in CdSe Nanocrystals under High Pressure. *The Journal of Chemical Physics* **1995,** *102*, 4642-4656.
7. Alivisatos, A. P., Perspectives on the Physical Chemistry of Semiconductor Nanocrystals. *The Journal of Physical Chemistry* **1996,** *100*, 13226-13239.
8. Chen, C.-C.; Herhold, A. B.; Johnson, C. S.; Alivisatos, A. P., Size Dependence of Structural Metastability in Semiconductor Nanocrystals. *Science* **1997,** *276*, 398-401.
9. Jacobs, K.; Zaziski, D.; Scher, E. C.; Herhold, A. B.; Paul Alivisatos, A., Activation Volumes for Solid-Solid Transformations in Nanocrystals. *Science* **2001,** *293*, 1803-1806.

10. Yu, W. W.; Wang, Y. A.; Peng, X., Formation and Stability of Size-, Shape-, and Structure-Controlled CdTe Nanocrystals: Ligand Effects on Monomers and Nanocrystals. *Chemistry of Materials* **2003,** *15*, 4300-4308.

11. Hines, M. A.; Scholes, G. D., Colloidal PbS Nanocrystals with Size-Tunable Near-Infrared Emission: Observation of Post-Synthesis Self-Narrowing of the Particle Size Distribution. *Advanced Materials* **2003,** *15*, 1844-1849.

12. McLaren, A.; Valdes-Solis, T.; Li, G.; Tsang, S. C., Shape and Size Effects of ZnO Nanocrystals on Photocatalytic Activity. *Journal of the American Chemical Society* **2009,** *131*, 12540-12541.

13. Mastronardi, M. L.; Maier-Flaig, F.; Faulkner, D.; Henderson, E. J.; Kübel, C.; Lemmer, U.; Ozin, G. A., Size-Dependent Absolute Quantum Yields for Size-Separated Colloidally-Stable Silicon Nanocrystals. *Nano Letters* **2012,** *12*, 337-342.

14. Yu, Y.; Fan, G.; Fermi, A.; Mazzaro, R.; Morandi, V.; Ceroni, P.; Smilgies, D.-M.; Korgel, B. A., Size-Dependent Photoluminescence Efficiency of Silicon Nanocrystal Quantum Dots. *The Journal of Physical Chemistry C* **2017,** *121*, 23240-23248.

15. Liu, C.; Zheng, L.; Song, Q.; Xue, Z.; Huang, C.; Liu, L.; Qiao, X.; Li, X.; Liu, K.; Wang, T., A Metastable Crystalline Phase in Two-Dimensional Metallic Oxide Nanoplates. *Angewandte Chemie International Edition* **2019,** *58*, 2055-2059.

16. Zhao, Q.; Hazarika, A.; Schelhas, L. T.; Liu, J.; Gaulding, E. A.; Li, G.; Zhang, M.; Toney, M. F.; Sercel, P. C.; Luther, J. M., Size-Dependent Lattice Structure and Confinement Properties in $CsPbI_3$ Perovskite Nanocrystals: Negative Surface Energy for Stabilization. *ACS Energy Letters* **2020,** *5*, 238-247.

17. Yang, F.; Wang, C.; Pan, Y.; Zhou, X.; Kong, X.; Ji, W. Surface Stabilized Cubic Phase of $CsPbI_3$ and $CsPbBr_3$ at Room Temperature. *Chinese Physics B* **2019,** *28*, 056402.

18. Yang, R. X.; Tan, L. Z., Understanding Size Dependence of Phase Stability and Band Gap in $CsPbI_3$ Perovskite Nanocrystals. *The Journal of Chemical Physics* **2020,** *152*, 034702.

19. Burschka, J.; Pellet, N.; Moon, S.-J.; Humphry-Baker, R.; Gao, P.; Nazeeruddin, M. K.; Grätzel, M., Sequential Deposition as a Route to High-Performance Perovskite-Sensitized Solar Cells. *Nature* **2013,** *499*, 316-319.

20. Chen, Q.; Zhou, H.; Hong, Z.; Luo, S.; Duan, H.-S.; Wang, H.-H.; Liu, Y.; Li, G.; Yang, Y., Planar Heterojunction Perovskite Solar Cells Via Vapor-Assisted Solution Process. *Journal of the American Chemical Society* **2014,** *136*, 622-625.

21. Green, M. A.; Ho-Baillie, A.; Snaith, H. J., The Emergence of Perovskite Solar Cells. *Nature Photonics* **2014,** *8*, 506-514.

22. Lin, Q.; Armin, A.; Nagiri, R. C. R.; Burn, P. L.; Meredith, P., Electro-Optics of Perovskite Solar Cells. *Nature Photonics* **2014,** *9*, 106.-112

23. Jeon, N. J.; Noh, J. H.; Yang, W. S.; Kim, Y. C.; Ryu, S.; Seo, J.; Seok, S. I., Compositional Engineering of Perovskite Materials for High-Performance Solar Cells. *Nature* **2015,** *517*, 476-480.

24. Swarnkar, A.; Marshall, A. R.; Sanehira, E. M.; Chernomordik, B. D.; Moore, D. T.; Christians, J. A.; Chakrabarti, T.; Luther, J. M., Quantum Dot–Induced Phase Stabilization of α-$CsPbI_3$ Perovskite for High-Efficiency Photovoltaics. *Science* **2016,** *354*, 92-95.

25. Xiao, Z.; Kerner, R. A.; Zhao, L.; Tran, N. L.; Lee, K. M.; Koh, T.-W.; Scholes, G. D.; Rand, B. P., Efficient Perovskite Light-Emitting Diodes Featuring Nanometre-Sized Crystallites. *Nature Photonics* **2017,** *11*, 108-115.

26. Zhao, L.; Yeh, Y.-W.; Tran, N. L.; Wu, F.; Xiao, Z.; Kerner, R. A.; Lin, Y. L.; Scholes, G. D.; Yao, N.; Rand, B. P., In Situ Preparation of Metal Halide Perovskite Nanocrystal Thin Films for Improved Light-Emitting Devices. *ACS Nano* **2017,** *11*, 3957-3964.

27. Lee, S.; Park, J. H.; Nam, Y. S.; Lee, B. R.; Zhao, B.; Di Nuzzo, D.; Jung, E. D.; Jeon, H.; Kim, J.-Y.; Jeong, H. Y.; Friend, R. H.; Song, M. H., Growth of Nanosized Single Crystals for Efficient Perovskite Light-Emitting Diodes. *ACS Nano* **2018,** *12*, 3417-3423.

28. Protesescu, L.; Yakunin, S.; Bodnarchuk, M. I.; Krieg, F.; Caputo, R.; Hendon, C. H.; Yang, R. X.; Walsh, A.; Kovalenko, M. V., Nanocrystals of Cesium Lead Halide Perovskites ($CsPbX_3$, X = Cl, Br, and I): Novel Optoelectronic Materials Showing Bright Emission with Wide Color Gamut. *Nano Letters* **2015,** *15*, 3692-3696.

29. Bekenstein, Y.; Koscher, B. A.; Eaton, S. W.; Yang, P.; Alivisatos, A. P., Highly Luminescent Colloidal Nanoplates of Perovskite Cesium Lead Halide and Their Oriented Assemblies. *Journal of the American Chemical Society* **2015,** *137*, 16008-16011.

30. Zhu, F.; Men, L.; Guo, Y.; Zhu, Q.; Bhattacharjee, U.; Goodwin, P. M.; Petrich, J. W.; Smith, E. A.; Vela, J., Shape Evolution and Single Particle Luminescence of Organometal Halide Perovskite Nanocrystals. *ACS Nano* **2015,** *9*, 2948-2959.

31. Di Stasio, F.; Christodoulou, S.; Huo, N.; Konstantatos, G., Near-Unity Photoluminescence Quantum Yield in $CsPbBr_3$ Nanocrystal Solid-State Films Via Postsynthesis Treatment with Lead Bromide. *Chemistry of Materials* **2017,** *29*, 7663-7667.

32. Rainò, G.; Becker, M. A.; Bodnarchuk, M. I.; Mahrt, R. F.; Kovalenko, M. V.; Stöferle, T., Superfluorescence from Lead Halide Perovskite Quantum Dot Superlattices. *Nature* **2018,** *563*, 671-675.

33. Akkerman, Q. A.; Abdelhady, A. L.; Manna, L., Zero-Dimensional Cesium Lead Halides: History, Properties, and Challenges. *The Journal of Physical Chemistry Letters* **2018,** *9*, 2326-2337.

34. Utzat, H.; Sun, W.; Kaplan, A. E. K.; Krieg, F.; Ginterseder, M.; Spokoyny, B.; Klein, N. D.; Shulenberger, K. E.; Perkinson, C. F.; Kovalenko, M. V.; Bawendi, M. G., Coherent Single-Photon Emission from Colloidal Lead Halide Perovskite Quantum Dots. *Science* **2019,** *363*, 1068-1072.

35. Nedelcu, G.; Protesescu, L.; Yakunin, S.; Bodnarchuk, M. I.; Grotevent, M. J.; Kovalenko, M. V., Fast Anion-Exchange in Highly Luminescent Nanocrystals of Cesium Lead Halide Perovskites ($CsPbX_3$, X = Cl, Br, I). *Nano Letters* **2015,** *15*, 5635-5640.

36. Pellet, N.; Teuscher, J.; Maier, J.; Grätzel, M., Transforming Hybrid Organic Inorganic Perovskites by Rapid Halide Exchange. *Chemistry of Materials* **2015,** *27*, 2181-2188.

37. Jang, D. M.; Park, K.; Kim, D. H.; Park, J.; Shojaei, F.; Kang, H. S.; Ahn, J.-P.; Lee, J. W.; Song, J. K., Reversible Halide Exchange Reaction of Organometal Trihalide Perovskite Colloidal Nanocrystals for Full-Range Band Gap Tuning. *Nano Letters* **2015,** *15*, 5191-5199.

38. Akkerman, Q. A.; D'Innocenzo, V.; Accornero, S.; Scarpellini, A.; Petrozza, A.; Prato, M.; Manna, L., Tuning the Optical Properties of Cesium Lead Halide Perovskite Nanocrystals by Anion Exchange Reactions. *Journal of the American Chemical Society* **2015,** *137*, 10276-10281.

39. Li, M.; Zhang, X.; Lu, S.; Yang, P., Phase Transformation, Morphology Control, and Luminescence Evolution of Cesium Lead Halide Nanocrystals in the Anion Exchange Process. *RSC Advances* **2016,** *6*, 103382-103389.

40. Creutz, S. E.; Crites, E. N.; De Siena, M. C.; Gamelin, D. R., Anion Exchange in Cesium Lead Halide Perovskite Nanocrystals and Thin Films Using Trimethylsilyl Halide Reagents. *Chemistry of Materials* **2018,** *30*, 4887-4891.

41. Wang, D.; Cavin, J.; Yin, B.; Thind, A. S.; Borisevich, A. Y.; Mishra, R.; Sadtler, B., Role of Solid-State Miscibility During Anion Exchange in Cesium Lead Halide Nanocrystals Probed by Single-Particle Fluorescence. *The Journal of Physical Chemistry Letters* **2020,** *11*, 952-959.

42. Cottingham, P.; Brutchey, R. L., Compositionally Dependent Phase Identity of Colloidal $CsPbBr_{3-x}I_x$ Quantum Dots. *Chemistry of Materials* **2016,** *28*, 7574-7577.

43. Haque, A.; Ravi, V. K.; Shanker, G. S.; Sarkar, I.; Nag, A.; Santra, P. K., Internal Heterostructure of Anion-Exchanged Cesium Lead Halide Nanocubes. *The Journal of Physical Chemistry C* **2018,** *122*, 13399-13406.

44. Koscher, B. A.; Bronstein, N. D.; Olshansky, J. H.; Bekenstein, Y.; Alivisatos, A. P., Surface- vs Diffusion-Limited Mechanisms of Anion Exchange in $CsPbBr_3$ Nanocrystal Cubes Revealed through Kinetic Studies. *Journal of the American Chemical Society* **2016,** *138*, 12065-12068.

45. Loiudice, A.; Strach, M.; Saris, S.; Chernyshov, D.; Buonsanti, R., Universal Oxide Shell Growth Enables in Situ Structural Studies of Perovskite Nanocrystals During the Anion Exchange Reaction. *Journal of the American Chemical Society* **2019,** *141*, 8254-8263.

46. Empedocles, S.; Bawendi, M., Spectroscopy of Single CdSe Nanocrystallites. *Accounts of Chemical Research* **1999,** *32*, 389-396.

47. Park, Y.-S.; Guo, S.; Makarov, N. S.; Klimov, V. I., Room Temperature Single-Photon Emission from Individual Perovskite Quantum Dots. *ACS Nano* **2015,** *9*, 10386-10393.

48. Orfield, N. J.; McBride, J. R.; Keene, J. D.; Davis, L. M.; Rosenthal, S. J., Correlation of Atomic Structure and Photoluminescence of the Same Quantum Dot: Pinpointing Surface and Internal Defects That Inhibit Photoluminescence. *ACS Nano* **2015,** *9*, 831-839.

49. Orfield, N. J.; McBride, J. R.; Wang, F.; Buck, M. R.; Keene, J. D.; Reid, K. R.; Htoon, H.; Hollingsworth, J. A.; Rosenthal, S. J., Quantum Yield Heterogeneity among Single Nonblinking Quantum Dots Revealed by Atomic Structure-Quantum Optics Correlation. *ACS Nano* **2016,** *10*, 1960-1968.

50. Rainò, G.; Nedelcu, G.; Protesescu, L.; Bodnarchuk, M. I.; Kovalenko, M. V.; Mahrt, R. F.; Stöferle, T., Single Cesium Lead Halide Perovskite Nanocrystals at Low Temperature: Fast Single-Photon Emission, Reduced Blinking, and Exciton Fine Structure. *ACS Nano* **2016,** *10*, 2485-2490.

51. Merdasa, A.; Tian, Y.; Camacho, R.; Dobrovolsky, A.; Debroye, E.; Unger, E. L.; Hofkens, J.; Sundström, V.; Scheblykin, I. G., "Supertrap" at Work: Extremely Efficient Nonradiative Recombination Channels in $MAPbI_3$ Perovskites Revealed by Luminescence Super-Resolution Imaging and Spectroscopy. *ACS Nano* **2017,** *11*, 5391-5404.

52. Gibson, N. A.; Koscher, B. A.; Alivisatos, A. P.; Leone, S. R., Excitation Intensity Dependence of Photoluminescence Blinking in $CsPbBr_3$ Perovskite Nanocrystals. *The Journal of Physical Chemistry C* **2018,** *122*, 12106-12113.

53. Freppon, D. J.; Men, L.; Burkhow, S. J.; Petrich, J. W.; Vela, J.; Smith, E. A., Photophysical Properties of Wavelength-Tunable Methylammonium Lead Halide Perovskite Nanocrystals. *Journal of Materials Chemistry C* **2017,** *5*, 118-126.

54. Yuan, G.; Ritchie, C.; Ritter, M.; Murphy, S.; Gómez, D. E.; Mulvaney, P., The Degradation and Blinking of Single $CsPbI_3$ Perovskite Quantum Dots. *The Journal of Physical Chemistry C* **2018,** *122*, 13407-13415.

55. Seth, S.; Ahmed, T.; Samanta, A., Photoluminescence Flickering and Blinking of Single $CsPbBr_3$ Perovskite Nanocrystals: Revealing Explicit Carrier Recombination Dynamics. *The Journal of Physical Chemistry Letters* **2018,** *9*, 7007-7014.

56. Boote, B. W.; Andaraarachchi, H. P.; Rosales, B. A.; Blome-Fernández, R.; Zhu, F.; Reichert, M. D.; Santra, K.; Li, J.; Petrich, J. W.; Vela, J.; Smith, E. A., Unveiling the Photo- and Thermal-Stability of Cesium Lead Halide Perovskite Nanocrystals. *ChemPhysChem* **2019,** *20*, 2647-2656.

57. Rainò, G.; Landuyt, A.; Krieg, F.; Bernasconi, C.; Ochsenbein, S. T.; Dirin, D. N.; Bodnarchuk, M. I.; Kovalenko, M. V., Underestimated Effect of a Polymer Matrix on the Light Emission of Single $CsPbBr_3$ Nanocrystals. *Nano Letters* **2019,** *19*, 3648-3653.

58. Routzahn, A. L.; Jain, P. K., Single-Nanocrystal Reaction Trajectories Reveal Sharp Cooperative Transitions. *Nano Letters* **2014,** *14*, 987-992.

59. Routzahn, A. L.; Jain, P. K., Luminescence Blinking of a Reacting Quantum Dot. *Nano Letters* **2015,** *15*, 2504-2509.

60. Brenner, T. M.; Rakita, Y.; Orr, Y.; Klein, E.; Feldman, I.; Elbaum, M.; Cahen, D.; Hodes, G., Conversion of Single Crystalline PbI_2 to $CH_3NH_3PbI_3$: Structural Relations and Transformation Dynamics. *Chemistry of Materials* **2016,** *28*, 6501-6510.

61. Karimata, I.; Kobori, Y.; Tachikawa, T., Direct Observation of Charge Collection at Nanometer-Scale Iodide-Rich Perovskites During Halide Exchange Reaction on $CH_3NH_3PbBr_3$. *The Journal of Physical Chemistry Letters* **2017,** *8*, 1724-1728.

62. Yin, B.; Cavin, J.; Wang, D.; Khan, D.; Shen, M.; Laing, C.; Mishra, R.; Sadtler, B., Fluorescence Microscopy of Single Lead Bromide Nanocrystals Reveals Sharp Transitions During Their Transformation to Methylammonium Lead Bromide. *Journal of Materials Chemistry C* **2019,** *7*, 3486-3495.

63. Wang, D.; Zhang, D.; Sadtler, B., Irreversibility in Anion Exchange between Cesium Lead Bromide and Iodide Nanocrystals Imaged by Single-Particle Fluorescence. *The Journal of Physical Chemistry C* **2020,** *124*, 27158-27168.

64. Yoshimura, H.; Yamauchi, M.; Masuo, S., In Situ Observation of Emission Behavior During Anion-Exchange Reaction of a Cesium Lead Halide Perovskite Nanocrystal at the Single-Nanocrystal Level. *The Journal of Physical Chemistry Letters* **2020,** *11*, 530-535.

65. Karimata, I.; Tachikawa, T., In Situ Exploration of the Structural Transition During Morphology- and Efficiency-Conserving Halide Exchange on a Single Perovskite Nanocrystal. *Angewandte Chemie International Edition* **2021,** *60*, 2548-2553.

66. Darmawan, Y. A.; Yamauchi, M.; Masuo, S., In Situ Observation of Emission Sites During the Halide Exchange Reaction in Single Cesium Lead Halide Perovskite Nanocrystals. *The Journal of Physical Chemistry C* **2022,** *126*, 2627-2633.

67. Dong, Y.; Qiao, T.; Kim, D.; Parobek, D.; Rossi, D.; Son, D. H., Precise Control of Quantum Confinement in Cesium Lead Halide Perovskite Quantum Dots Via Thermodynamic Equilibrium. *Nano Letters* **2018,** *18*, 3716-3722.

68. Peng, L.; Dutta, A.; Xie, R.; Yang, W.; Pradhan, N., Dot–Wire–Platelet–Cube: Step Growth and Structural Transformations in $CsPbBr_3$ Perovskite Nanocrystals. *ACS Energy Letters* **2018,** *3*, 2014-2020.

69. Sugimoto, T., Preparation of Monodispersed Colloidal Particles. *Advances in Colloid and Interface Science* **1987,** *28*, 65-108.

70. Akkerman, Q. A.; Nguyen, T. P. T.; Boehme, S. C.; Montanarella, F.; Dirin, D. N.; Wechsler, P.; Beiglböck, F.; Rainò, G.; Erni, R.; Katan, C.; Even, J.; Kovalenko, M. V., Controlling the Nucleation and Growth Kinetics of Lead Halide Perovskite Quantum Dots. *Science* **2022,** *377*, 1406-1412.

71. Maes, J.; Balcaen, L.; Drijvers, E.; Zhao, Q.; De Roo, J.; Vantomme, A.; Vanhaecke, F.; Geiregat, P.; Hens, Z., Light Absorption Coefficient of $CsPbBr_3$ Perovskite Nanocrystals. *The Journal of Physical Chemistry Letters* **2018,** *9*, 3093-3097.

72. Scharf, E.; Krieg, F.; Elimelech, O.; Oded, M.; Levi, A.; Dirin, D. N.; Kovalenko, M. V.; Banin, U., Ligands Mediate Anion Exchange between Colloidal Lead-Halide Perovskite Nanocrystals. *Nano Letters* **2022,** *22*, 4340-4346.

73. Abdel-Latif, K.; Epps, R. W.; Kerr, C. B.; Papa, C. M.; Castellano, F. N.; Abolhasani, M., Facile Room-Temperature Anion Exchange Reactions of Inorganic Perovskite Quantum Dots Enabled by a Modular Microfluidic Platform. *Advanced Functional Materials* **2019,** *29*, 1900712.

74. Son, D. H.; Hughes, S. M.; Yin, Y.; Paul Alivisatos, A., Cation Exchange Reactions in Ionic Nanocrystals. *Science* **2004,** *306*, 1009-1012.

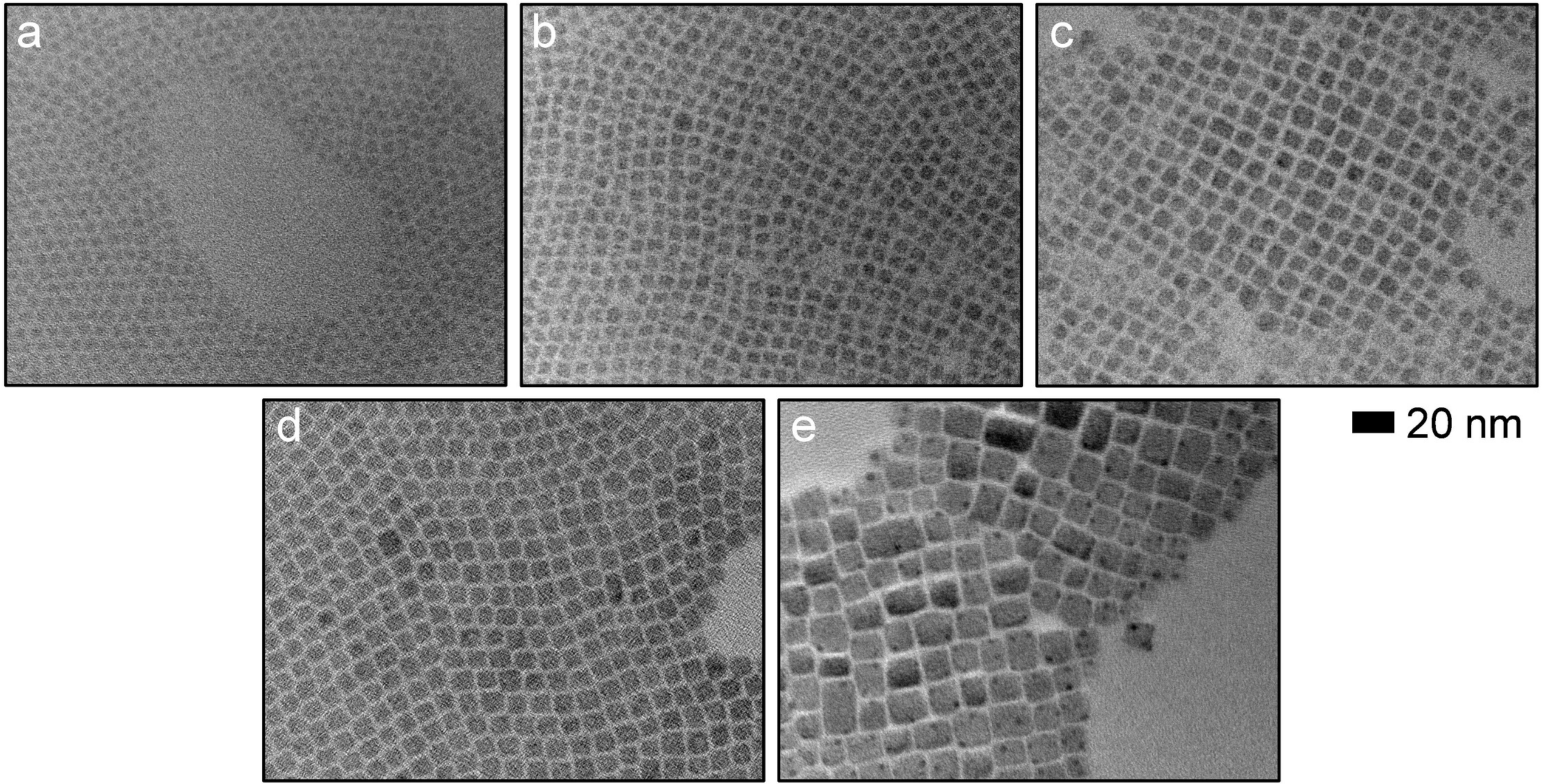
a
b
c
d
e
20 nm

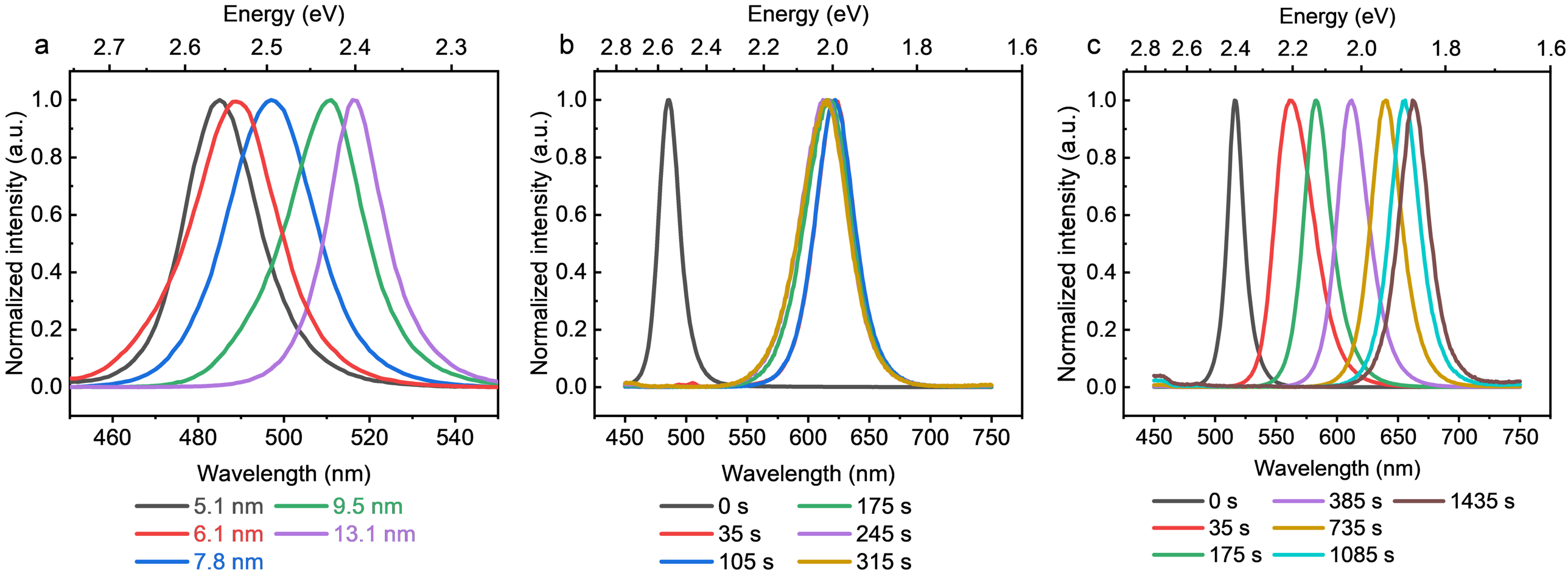
a
Energy (eV)
2.7
2.6
2.5
2.4
2.3
Normalized intensity (a.u.)
1.0
0.8
0.6
0.4
0.2
0.0
460
480
500
520
540
Wavelength (nm)
5.1 nm
9.5 nm
6.1 nm
13.1 nm
7.8 nm
b
Energy (eV)
2.8
2.6
2.4
2.2
2.0
1.8
1.6
Normalized intensity (a.u.)
450
500
550
600
650
700
750
Wavelength (nm)
0 s
175 s
35 s
245 s
105 s
315 s
c
Energy (eV)
2.8
2.6
2.4
2.2
2.0
1.8
1.6
Normalized intensity (a.u.)
450
500
550
600
650
700
750
Wavelength (nm)
0 s
385 s
1435 s
35 s
735 s
175 s
1085 s

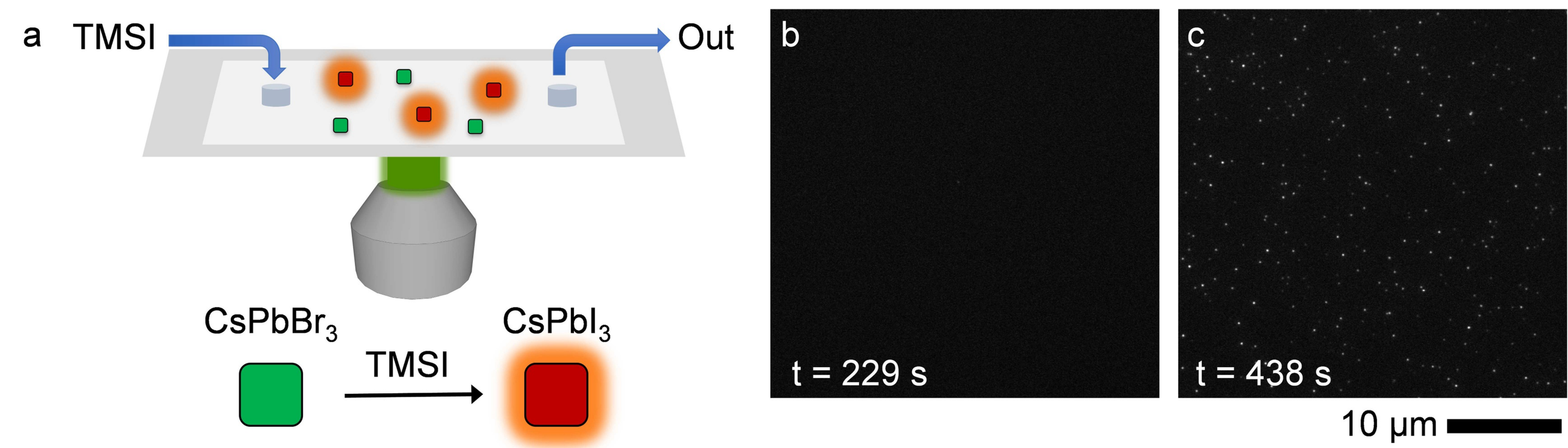
a
TMSI
Out
CsPbBr3
TMSI
CsPbI3
b
t = 229 s
c
t = 438 s
10 μm

a

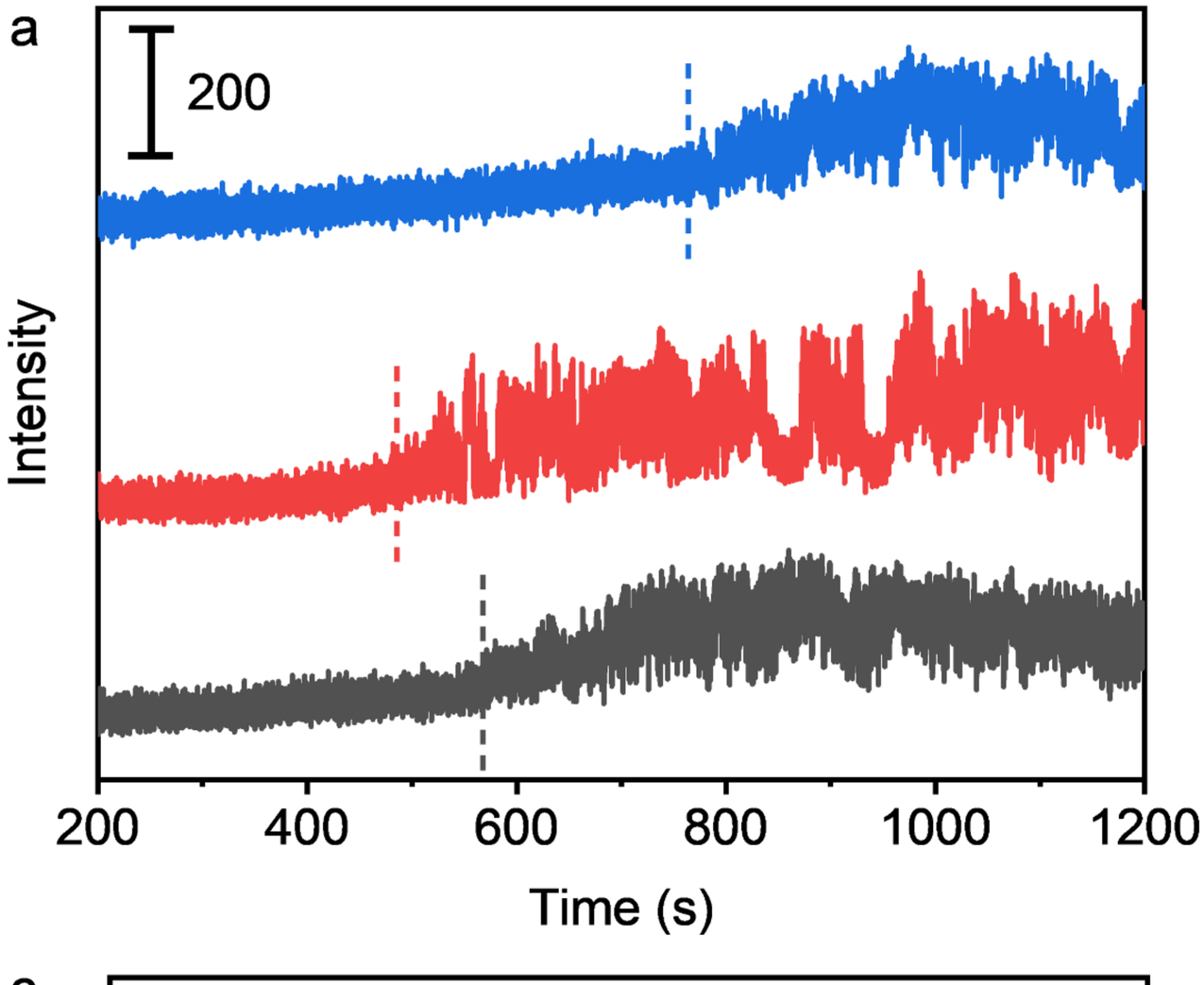
200
Intensity
200
400
600
800
1000
1200
Time (s)

b

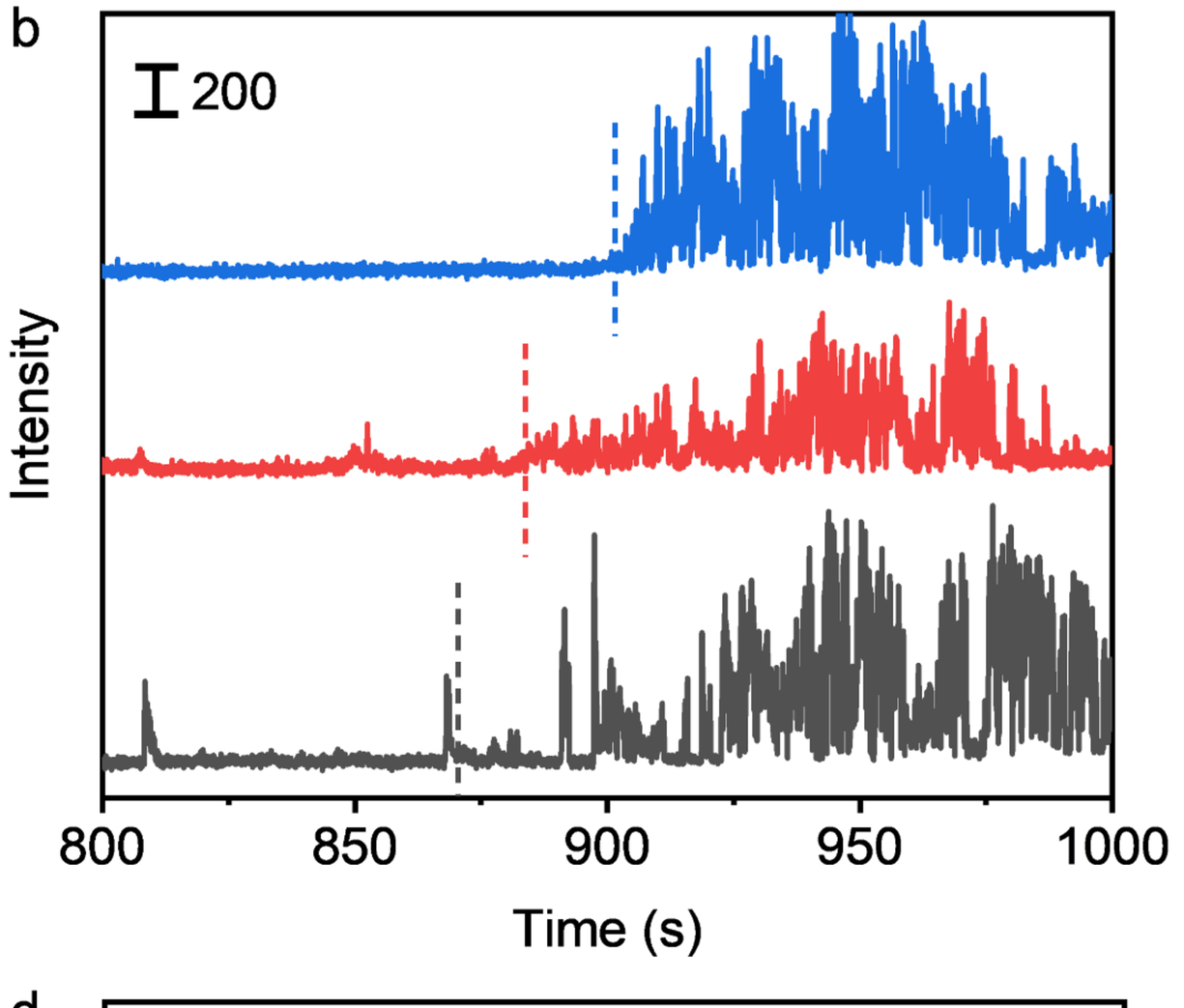
200
Intensity
800
850
900
950
1000
Time (s)

c

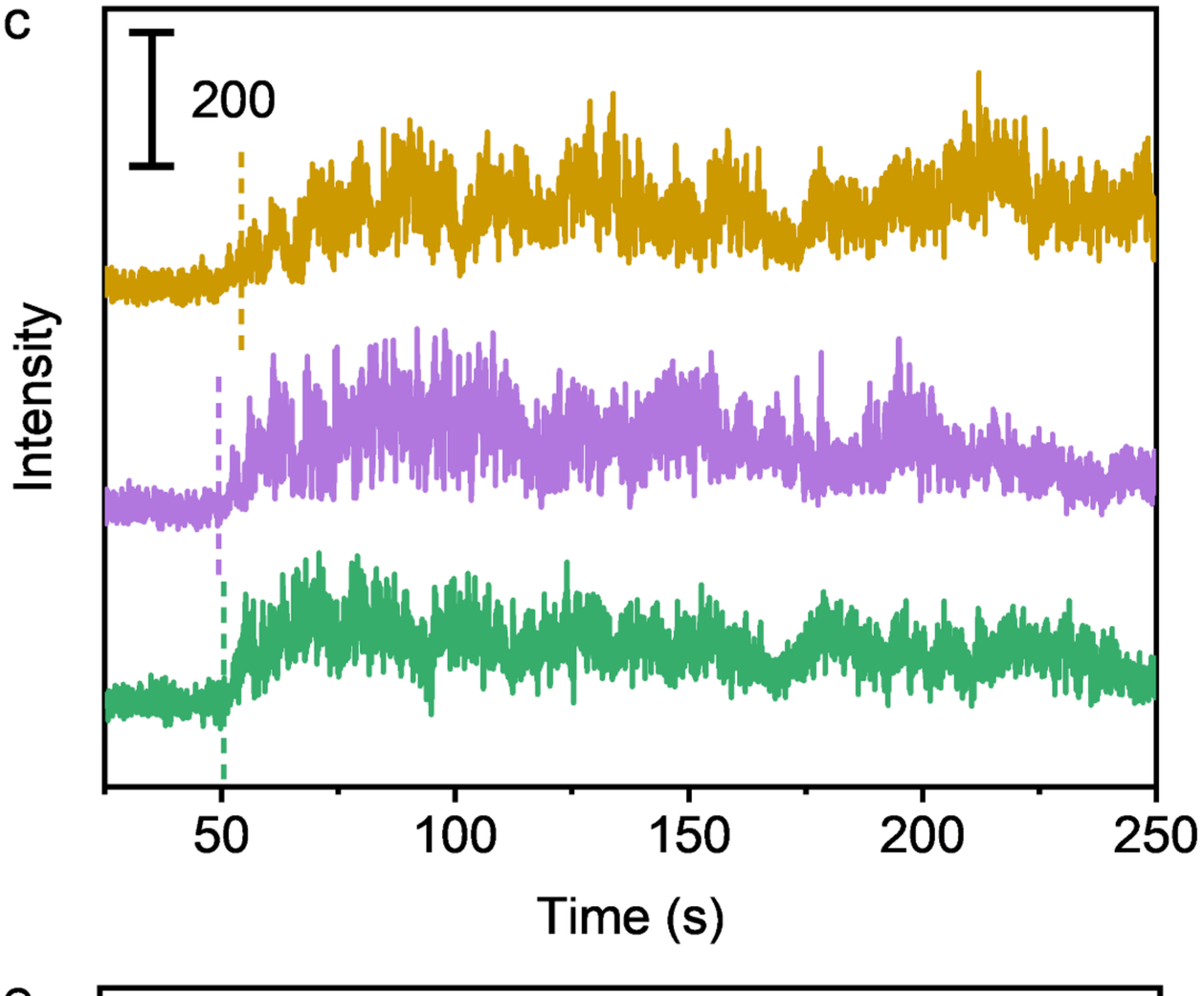
200
Intensity
50
100
150
200
250
Time (s)

d

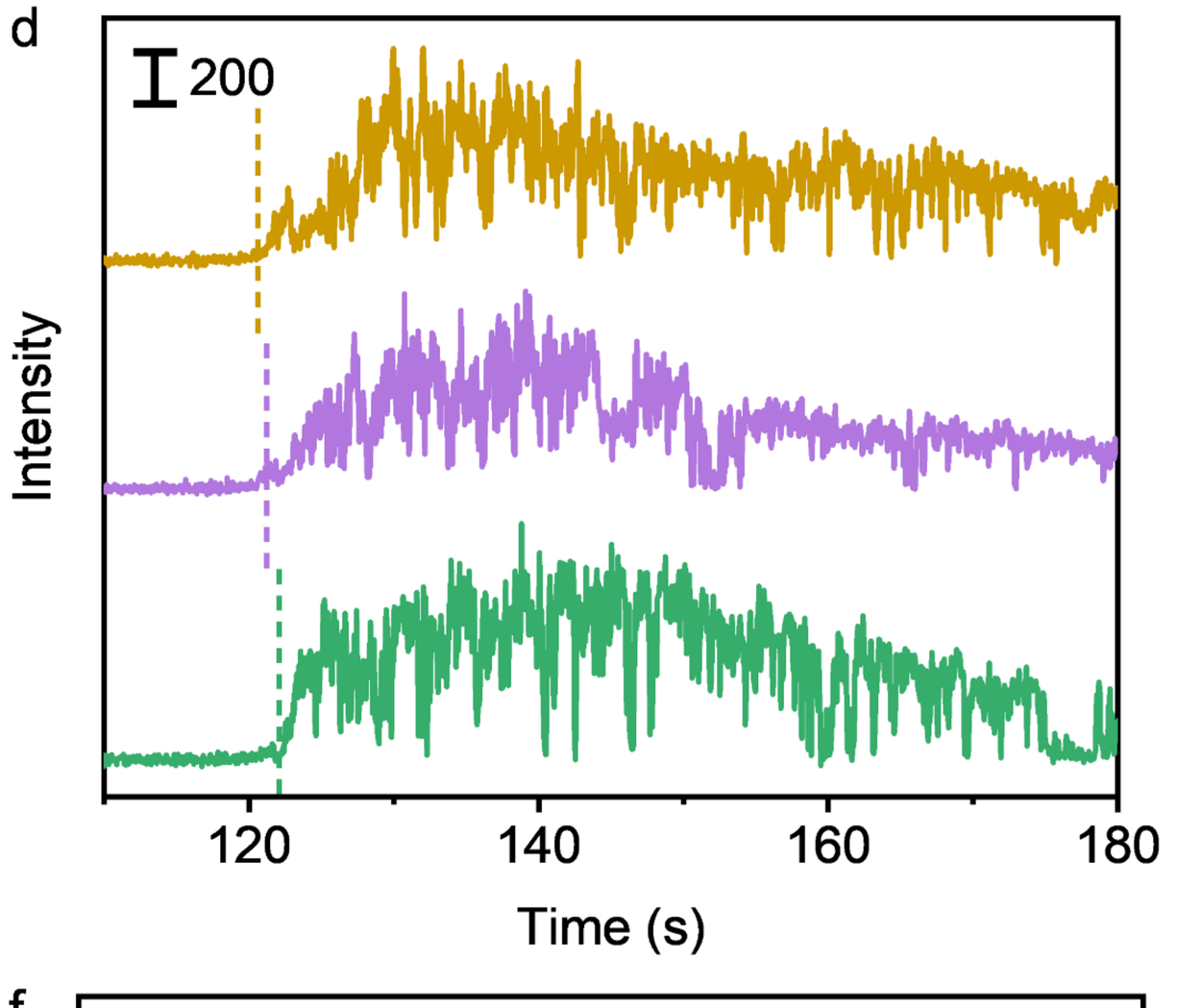
200
Intensity
120
140
160
180
Time (s)

e

200
50 μM
5 μM
Intensity
-25
0
25
50
75
100
125
150
175
200
Time (s)

f

200
50 μM
5 μM
Intensity
-40
-20
0
20
40
60
80
100
Time (s)

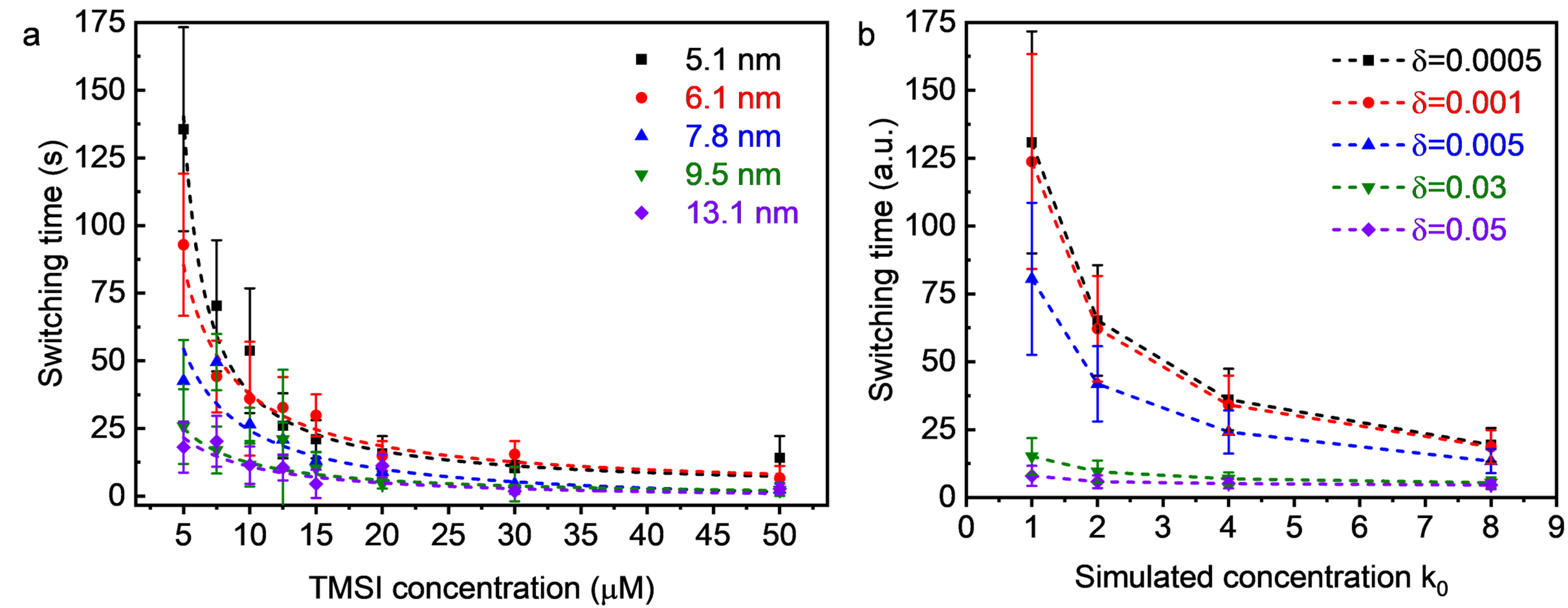
a
Switching time (s)
TMSI concentration (μM)
5.1 nm
6.1 nm
7.8 nm
9.5 nm
13.1 nm
b
Switching time (a.u.)
Simulated concentration k0
δ=0.0005
δ=0.001
δ=0.005
δ=0.03
δ=0.05